THE JOURNAL OF PHYSICAL CHEMISTRY C

Article

pubs.acs.org/JPCC

Pressure-enhanced Insulating State and Trigonal Distortion Relaxation in Geometrically Frustrated Pyrochlore $Eu_2Sn_2O_7$

Yongsheng Zhao,[†,‡] Wenge Yang,[*,‡,$] Nana Li,[‡] Yan Li,[§] Ruilian Tang,[‡] Hui Li,[†] Hongyu Zhu,[†] Pinwen Zhu,[†] and Xin Wang[*,†]

[†]State Key Laboratory of Superhard Materials, Jilin University, Changchun 130012, China

[‡]Center for High Pressure Science and Technology Advanced Research (HPSTAR), Shanghai 201203, China

[$]High Pressure Synergetic Consortium (HPSynC), Geophysical Laboratory, Carnegie Institution of Washington, Argonne, Illinois 60439, United States

[§]College of Physics, Jilin University, Changchun 130012, China

ABSTRACT: The geometrically frustrated pyrochlore $Eu_2Sn_2O_7$ is an insulator with slight trigonal lattice distortion at ambient condition. High pressure is applied to this system to investigate the responses of structural evolution, optical emission and electrical transport properties. *In situ* high pressure synchrotron X-ray diffraction, Raman spectroscopy, and photoluminescence studies are performed in $Eu_2Sn_2O_7$ up to 31.2 and 34.1 GPa, respectively. The abrupt change of the oxygen atomic position without breaking the crystal symmetry is accompanied by disappearing of Raman mode involving SnO_6 octahedron distortion around 17.8 GPa. It indicates a pressure-induced second-order iso-structural transition, which suppresses the trigonal distortion in the SnO_6 octahedron but enhances the local symmetry distortion of EuO_8 hexahedron. Anomalous luminescence of the Eu^{3+} 4f−4f transition is observed, which confirms the enhancement of EuO_8 hexahedral distortion at high pressure region. *In situ* high-pressure electrical transport property is measured by alternating current (AC) impedance spectroscopy up to 32.5 GPa. A rapid increase in resistance with gain of 4 orders of magnitude by applied pressure is observed until 16.6 GPa, and it is followed by a slight decreasing to the highest pressure measured here. All these observations indicate a pressure-enhanced trigonal lattice distortion before the transition pressure, and thus it will enlarge an opening gap at the Fermi energy, followed by releasing distortion at higher pressures.

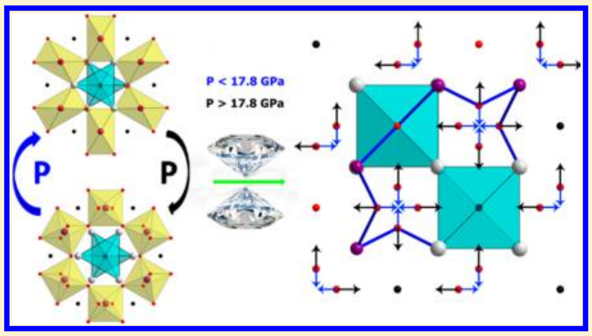

■ INTRODUCTION

Insulating rare-earth stannate pyrochlores $R_2Sn_2O_7$ (R = rare-earth ion) have many potential applications with their complex magnetic behaviors, arising from their geometrical frustration configuration.[1] Over several decades, the rare-earth titanates and stannates have been widely investigated to search for their unusual ground states. For example, frustrated pyrochlores $R_2Ti_2O_7$ exhibited exotic magnetic behaviors such as dipolar spin ice, spin liquid phases, first-order transition in the spin dynamics, and complex antiferromagnetic (AFM) orders.[2−5] In these materials, the type of magnetic order depends on the balance between antiferromagnetic exchange, dipolar, and crystal field energies.[6] The stannates $R_2Sn_2O_7$ have the same crystal structure and the susceptibility data as the titanates, suggesting a potential great variety of the magnetic behaviors.[7,8] $Dy_2Sn_2O_7$ and $Ho_2Sn_2O_7$ exhibited dipolar spin ices behaviors like their Ti-based compounds, while $Pr_2Sn_2O_7$ showed dynamic spin ice and $Tb_2Sn_2O_7$ showed an ordered spin ice.[9,10] Other rare earth pyrochlores like $Er_2Sn_2O_7$ could exhibit a liquid-like ground state.[11] Therefore, the Sn-type pyrochlores with many fantastic magnetic ground states attract broad fundamental studies over last decades.

Pressure as one of the fundamental state parameters has been widely used to tune the structure−property of materials, from superhard materials to high-temperature surperconductors.[12,13] Under high pressure, the pyrochlore materials can become surpercondutors, and undergo magnetic transitions and metal−insulator transitions.[14−16] Pressure is also applied to generate magnetic monopole dimers in spin ice compound.[17] For magnetic pyrochlore oxide $Tb_2Ti_2O_7$, pressure could induce crystallization from the pristine spin liquid state, and destroy this delicate balance thus reducing this frustration character above 9 GPa.[18,19] This was believed to be the original driving force of the development of magnetic correlations at high pressure and low temperature. It has been confirmed that the application of pressure can relieve the frustration via the structural distortion.

Rare earth Eu^{3+} and Tb^{3+} ions are often used as doping elements to many host materials like BaFCl:Eu^{3+}, YF_3:Eu^{3+}, and Y_2O_3:Eu^{3+}/Tb^{3+} to improve their luminescence.[20−22] Stannate

Received: March 3, 2016
Revised: April 21, 2016
Published: April 21, 2016

DOI: 10.1021/acs.jpcc.6b02246
J. Phys. Chem. C 2016, 120, 9436−9442

pyrochlore $Eu_2Sn_2O_7$ as a self-activated luminescence material, can act as not only a host crystal for doping activator but also a phosphor host material which is applied in flat-panel displays.[23,24] However, most of these researches on $A_2Sn_2O_7$ are limited to ambient pressure.[25,26]

In order to achieve comprehensive understanding on the pressure effects on $A_2Sn_2O_7$ stannate pyrochlores, the information about the structural evolution at high pressure is needed. In this paper, the selected pyrochlore $Eu_2Sn_2O_7$ is first synthesized using the high pressure and high temperature (HPHT) method with a much better crystallinity quality. *In situ* high pressure X-ray diffraction (XRD), Raman spectroscopy, photoluminescence (PL) spectroscopy and AC impedance spectroscopy are carried out to investigate the structural, optical, and electrical transport properties of $Eu_2Sn_2O_7$. It is shown that the lattice stability is significantly altered by pressure accompanied by the anomalous luminescence of the Eu^{3+} 4f−4f transition and increasing resistance of 4 orders of magnitude. It exhibits an uncommon pressure-enhanced insulating state, which is believed largely to connect with the EuO_8 and SnO_6 polyhedral distortions and frustration releasing, and it results in electronic band gap opening. The comprehensive understanding of the lattice, optical, and electrical evolution with pressure in pyrochlore oxides may shed light on the novel functional materials design and synthesis with advanced properties.

■ EXPERIMENTAL DETAILS

Synthesis Preparation. Samples of $Eu_2Sn_2O_7$ were synthesized under HPHT conditions. The high purity powders SnO_2 and Eu_2O_3 (99.9% in purity from Alfa Aesar) were uniformly mixed with 2:1 molar ratio in an agate mortar, and pressed into a disk with 6 mm in diameter and 2 mm in height. The disk was compressed to 5.2 GPa in a cubic anvil high-pressure apparatus at 1573 K for 30 min. The as-synthesized materials were checked with a Rigaku X-ray diffractometer with Cu Kα radiation (λ = 1.5418 Å) to make sure of the high quality of the pure cubic phase of $Eu_2Sn_2O_7$.

High Pressure XRD, Raman, and Photoluminescence Spectroscopy. The *in situ* high-pressure XRD measurements were performed with an angle-dispersive synchrotron source (λ = 0.4049 Å) at beamline X17C of the National Synchrotron Light Source, Brookhaven National Laboratory. Diamond anvil cell (DAC) was used to generate high pressure, and the fine powder of $Eu_2Sn_2O_7$ was loaded into a precompressed and drilled stainless steel gasket with a methanol/ethanol/water mixture (16:3:1) as pressure-transmitting medium. The high pressure Raman spectroscopy and photoluminescence spectra were measured with a 532 nm excitation laser at the Center for High Pressure Science and Technology Advance Research (HPSTAR). Pressure was calibrated by the ruby luminescence method.[27]

High Pressure Transport Measurement. The Van der Pauw four-probe method was utilized in DAC for electric properties measurement under high pressure. The fabricated process of the detecting microcircuit has been reported in previous publication.[28] The measurements of ac impedance spectroscopy in the frequency range of 0.01 Hz to 10 MHz at pressures up to 32.5 GPa were carried out by using a Solartron 1260 impedance analyzer equipped with Solartron 1296 dielectric interface. The applied ac voltage was 0.2 V and no pressure medium was used in the resistance measurements.

■ RESULTS AND DISCUSSION

Crystal Structure. At ambient condition, pyrochlore $Eu_2Sn_2O_7$ belonging to the $A_2B_2O_6O'$ compounds crystallizes in the space group $Fd\bar{3}m$ (SG#227) with two D_{3d} symmetry polyhedra.[1] The A-cation occupies the 16*c* Wyckoff position with eight coordination and is surrounded with a distorted cubic coordinated polyhedron, while the B-cation occupies the 16*d* position with six coordination in a distorted octahedron. The atomic arrangement is shown in Figure 1a. There are two

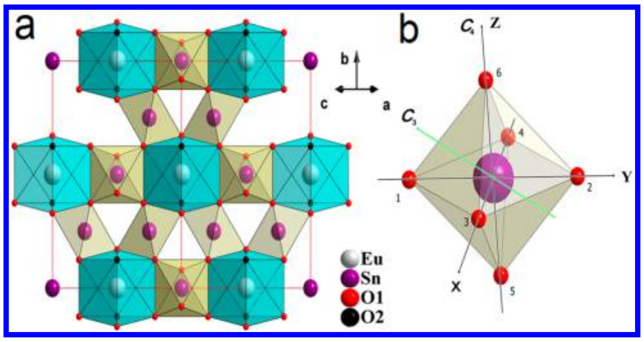

Figure 1. Crystal structure of the geometrically frustrated pyrochlore $Eu_2Sn_2O_7$. (a) Atomic arrangement in a unit cell with space group $Fd\bar{3}m$, the EuO_8 and SnO_6 polyhedron are shaded in light blue and light yellow, respectively. (b) Perfect SnO_6 octahedron. A trigonal distortion is induced by compression or elongation of the surrounding oxygen octahedron along a C_3 or C_4 symmetry axis (z axis), respectively. The C_3 symmetry axis is across the planes of O_{136} and O_{245} (or its equivalent axes).

types of oxygen sites: the 48*f* oxygen (O1) at the octahedral vertices connected to two B^{4+} and two A^{3+} cations; the 8*b* oxygen (O2) at the tetrahedral vertices connected to A^{3+} cations only.[29] The SnO_6 octahedra are distorted either in an elongated or a compressed arrangement along the 3-fold axis (C_3) as shown in Figure 1b, which only depends on the free O_{48f} position parameter, x.[30] When x = 0.3125, SnO_6 forms a regular octahedron; when x = 0.375, the EuO_8 hexahedron forms a perfect cube; when 0.3125 < x < 0.375, both SnO_6 octahedron and EuO_8 hexahedron are distorted. At ambient pressure, the obtained structural parameters of a = 10.4561(1) Å, and x = 0.3308(4) from the as-synthesized $Eu_2Sn_2O_7$ are deduced from X-ray powder diffraction with the GSAS Rietveld refinement.[31] These values are consistent with the previous report.[32]

***In Situ* High Pressure XRD.** In order to check the structural stability and lattice evolution under high pressure, we have conducted the *in situ* synchrotron XRD on the powder $Eu_2Sn_2O_7$ sample in DAC at room temperature. Figure 2a shows several typical XRD patterns of $Eu_2Sn_2O_7$ up to 31.2 GPa. All the diffraction peaks shift to higher angles with the increase of pressure, and no crystallographic symmetry change is observed up to the highest pressure. Nevertheless, the detailed analysis yields the structural parameters of unit cell volume and x parameter as a function of applied pressure. Since the fractional coordinate x of the oxygen atom at the 48*f* site shows a sudden drop at 17.8 GPa as shown in the inset of Figure 2b, the pressure-dependent volume can be divided into two regions at this critical pressure. As shown in Figure 2b, third-order Birch−Murnaghan equation of state[33] has been applied to fit the data before and after 17.8 GPa, and it yields B = 170 GPa with B' = 8.0 at the low pressure side and B = 285

DOI: 10.1021/acs.jpcc.6b02246
J. Phys. Chem. C 2016, 120, 9436−9442

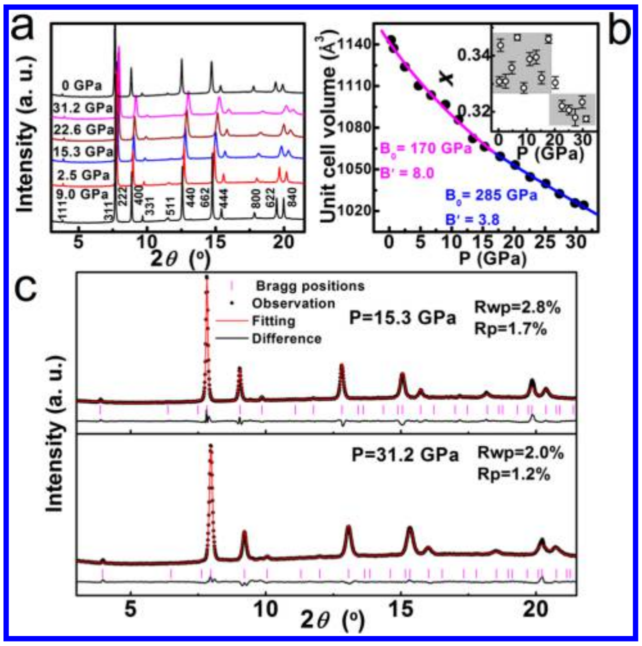

Figure 2. High pressure structural evolution probed by synchrotron XRD at ambient temperature. (a) Angle dispersive XRD patterns of $Eu_2Sn_2O_7$ at selected pressures with incident wavelength of $\lambda = 0.4049$ Å. (b) Unit cell volume of $Eu_2Sn_2O_7$ as a function of pressure. The data are divided into two regions with third-order Birch−Murnaghan equation of state fitting. The inset shows the variation of positional parameter x with increasing pressure and a sudden drop above 17.8 GPa. (c) Two representative Rietveld refinements of XRD patterns at pressures of 15.4 and 31.2 GPa obtained by using the GSAS program.

GPa with $B' = 3.8$ at the high pressure side. The large $B' = 8.0$ reflects the pronounced anisotropic compressibility at lower pressure region and a nearly 67% increase in bulk modulus indicates a much rigid framework formed at higher pressure region. The similar changes have been reported in other pyrochlores $Tb_2Ti_2O_7$ and $La_2Zr_2O_7$, which happened near 9 GPa, and it was attributed to the TiO_6 (ZrO_6) octahedron rearrangement and cation disorder.[19,34] Two representative GSAS Reitveld refinements at low pressure and high pressure region are shown in Figure 2c to demonstrate the good fittings to the experimental patterns. The concurrent changes of the bulk modulus and fractional coordinate x without volume discontinuity suggest a second-order isostructural transition under high pressure.

The pressure dependences of bond lengths, bond angles, and the normalized volumes of the SnO_6 octahedron are shown in Figure 3. A clear change can be seen at 17.8 GPa. As shown in the inset of Figure 3c, the long O1−O1 bonding distance in the SnO_6 octahedron is quickly compressed and approaches to the short O1−O1 bonding distance when the pressure is beyond 17.8 GPa. It leads to a large releasing of the SnO_6 octahedron distortion and forming a regular octahedron. In Figure 4a, the structural deformation of $Eu_2Sn_2O_7$ after applying pressure is displayed. The yellow cage-like polyhedron represents the SnO_6 octahedron and each Sn^{4+} ion is coordinated by six oxygen anions (O1) which keep equal distance from the central Sn^{4+} cation. The blue one represents the Eu_4O octahedron with oxygen O2 in the center. Obviously, the SnO_6 octahedral distortion will be seriously enhanced along the C_3 rotary axis below 17.8 GPa as shown in Figure 4b, and this distortion is in accordance with Jahn−Teller (JT) distortion like in $LaMnO_3$.[35] For $x = 0.3125$, the oxygen ligands around each Sn^{4+} ion form a regular octahedron, presenting a perfect local cubic crystal field, and the deviation of x from this ideal value generates a trigonal crystal field leading to a destabilization of the orbital order. Our XRD results have revealed that a large deviation of x from the prefect value at low pressure suggesting compressive trigonal distortion of the SnO_6 octahedron, while the distinct drop of parameter x from 0.345 to 0.319 indicates that the trigonal distortion is largely suppressed by pressure after the transition. In order to further analyze the relation between trigonal distortion and crystal lattice, we have compared the compression rates of the normalized volumes of distorted SnO_6 octahedron and unit-cell, as shown in Figure 3c. A significant decrease with pressure in octahedron volume, which

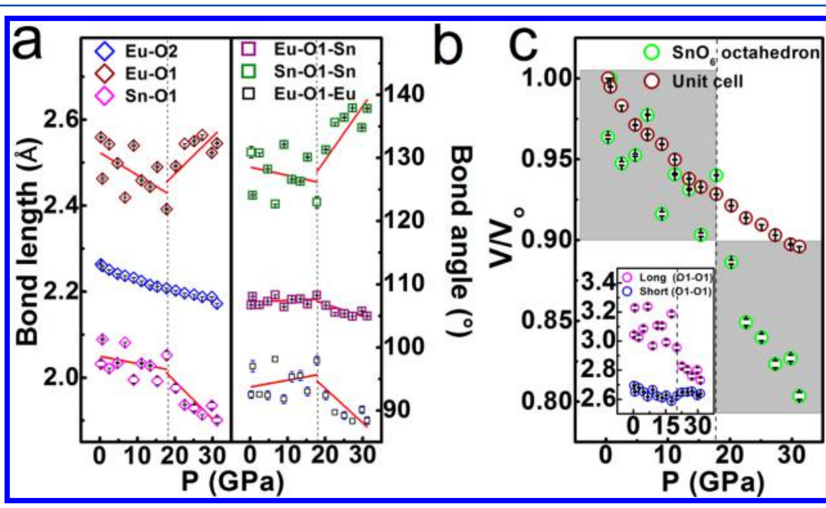

Figure 3. Evolutions of bonding angles and bond distances in SnO_6 and EuO_8 polyhedra under high pressure. Pressure dependences of bond lengths (a) and bond angles (b) in $Eu_2Sn_2O_7$. Obviously, significant changes in slope occurred at 17.8 GPa, except for the Eu−O2 bonding. With further increasing pressure, the Sn−O−Sn bond angle is becoming closer to linear configuration, which implies that the SnO_6 octahedral trigonal distortion is released above 17.8 GPa. (c) Normalized volumes of the SnO_6 and unit cell as a function of pressure. Obviously, the relative compression of the distorted SnO_6 octahedron is faster than that of the unit cell above 17.8 GPa. The inset shows the changes of two O1−O1 bonding distances at high pressure, from which one can see that the long (pink) O1−O1 distance is approaching the short (blue) O1−O1 distance beyond 17.8 GPa.

DOI: 10.1021/acs.jpcc.6b02246
J. Phys. Chem. C 2016, 120, 9436−9442

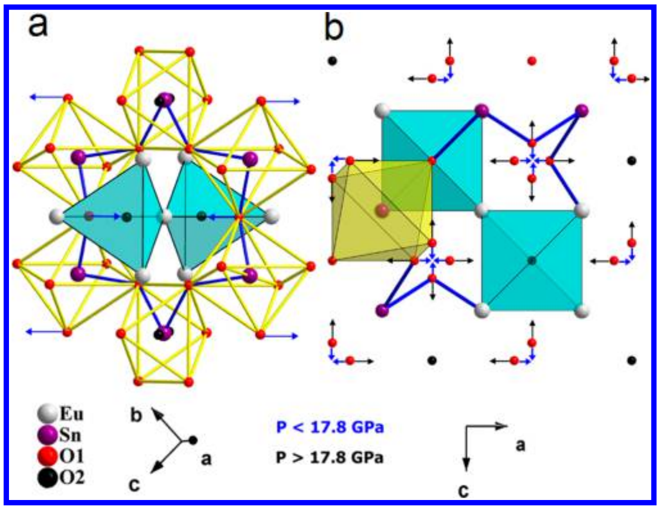

Figure 4. Schematic of the SnO_6 and EuO_8 polyhedron distortion. (a) SnO_6 octahedral and Eu_4O tetrahedral structures. The yellow cage-like polyhedron represents the SnO_6 octahedron and the blue one represents Eu_4O tetrahedron. (b) Oxygen atom position changes depend on pressure. Arrows show the oxygen atomic shift direction. Obviously, below 17.8 GPa, the SnO_6 octahedral trigonal distortion is seriously compressed along the C_3 rotation axis with increasing pressure. Above 17.8 GPa, shifting of O1−O1 bonding distance makes the SnO_6 octahedron close to a perfect octahedron with increasing pressure.

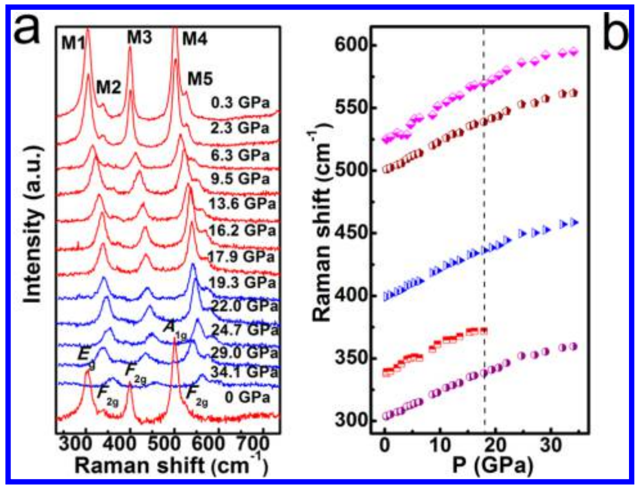

Figure 5. Study of Raman spectroscopy under high pressure. (a) Selected Raman spectra at different pressures. (b) Shifts of Raman mode frequencies with increasing pressure. The M2 mode is assigned to a triply degenerate F_{2g} mode, which disappears at 19.3 GPa.

implies the octahedral tilting along C_3 symmetry axis, signifies the released trigonal distortion above 17.8 GPa, and the released distortion can compensate the SnO_6 octahedral volume decreasing. It can be easily understood by the changes of two different O1−O1 distances in the SnO_6 octahedron as shown in the inset of Figure 3c, since pressure drives both O1−O1 bonds to become nearly equal. Similar interpretations for such changes including SnO_6 octahedral rearrangement and forming domains with pressure were reported.[19,35] In the trigonal distortion, the local symmetry group around transition metal site reduces from cubic O_h to D_{3d} in pyrochlore and the degenerate t_{2g} orbitals split into a singlet a_{1g} state and a doublet e_g state.[30,36] Therefore, the SnO_6 octahedral distortion is enhanced with pressure and reaches the maximum at 17.8 GPa, then the distortion is released beyond 17.8 GPa. It is also accompanied by the anomalous change in the normalized volumes of SnO_6 above 17.8 GPa, and this suggests that the local structural symmetry may change due to the lattice distortion but the cubic crystal lattice remains the same.

Raman Spectroscopy at High Pressure. Raman spectroscopy is sensitive to the detection of local bonding distance and bonding angle. Here, the study of high pressure Raman spectroscopy is investigated in the similar pressure range. At ambient condition, five Raman modes are observed at 304, 338, 400, 499, and 537 cm^{-1}, which correspond to E_g, A_{1g}, and $3F_{2g}$, and are labeled as M1, M2, M3, M4, and M5 as shown in Figure 5a. The locations of these modes were in consistence with previous ambient pressure Raman studies of $A_2Sn_2O_7$.[37−40] According to interatomic distance vs force constant variation, the modes M1 and M4 are identified as E_g and A_{1g}, respectively. The other Raman modes of M2, M3, and M5 are assigned to F_{2g} modes. The Raman-active modes are involved with the movement of oxygen atoms, which are due to Eu−O stretching, O−Eu−O bending, O−O stretching, and O−Sn−O bending and stretching. With increasing pressure, all Raman modes move to higher wavenumber as shown in Figure 5b, representing the regular compression behavior. The M2 mode became weaker and disappeared at 19.3 GPa. As discussed in $Gd_2Ti_2O_7$, similar change in anion position or a distortion in the octahedral lattice may be responsible for the disappearing of mode M2. In general, tetragonal or orthorhombic distortion is induced by E_g phonon modes and trigonal distortion is driven by F_{2g} phonon modes.[30] Here the disappeared F_{2g} mode (M2) at 19.3 GPa is corroborated with the change of its bulk modulus as detected by XRD, which provides additional evidence on the pressure induced trigonal lattice distortion at high pressure regions. After releasing pressure, these Raman-active modes come back, and hence the subtle structural change is reversible.

Photoluminescence Spectroscopy at High Pressure. The $Eu^{2/3+}$ ion has been used as doping particles in many host crystals as a phosphor due to its excellent luminescence properties.[23,41−44] Besides, it is also used to investigate the local symmetry of the cations because the $^5D_0$ and $^7F_0$ level of Eu^{3+} ion are nondegenerated which can be used to detect the crystal field splitting. The diffuse reflection spectra have one broad absorption peak at the wavelength of 630 nm that is originated from the 4f−4f transitions of Eu^{3+} ions. Since the local symmetry around Eu^{3+} is influenced by such transitions, it is sensitive to detect the structural changes.[21] Figure 6a shows the PL spectra of $Eu_2Sn_2O_7$ with pressure as excited by a 532 nm laser. The peak at 579 nm is from the Eu^{3+} ion $^5D_0 \rightarrow {}^7F_0$ transition. The peaks of 588, 592, and 596 nm correspond to $^5D_0 \rightarrow {}^7F_1$ (magnetic dipole) transition and are called as orange luminescence. Two strongest peaks at 612 and 617 nm correspond to $^5D_0 \rightarrow {}^7F_2$ (electric dipole) transition, and are called as red luminescence. Because of the selection rules and transition probabilities, if the Eu^{3+} ion sites are in inversion symmetry, the $^5D_0 \rightarrow {}^7F_2$ transition is forbidden. However, in this work, $^5D_0 \rightarrow {}^7F_2$ transition has even stronger intensity than $^5D_0 \rightarrow {}^7F_1$ transition, which is quite different from most Eu^{3+}-doped crystalline compounds. We speculate that the local symmetry of Eu^{3+} site is slightly distorted to the lower D_{3d} symmetry.[20,22,45] Figure 6b shows the emission intensity ratio of Orange to Red (O/R) ($^5D_0 \rightarrow {}^7F_1/{}^5D_0 \rightarrow {}^7F_2$) of $Eu_2Sn_2O_7$ as a function of pressure. The O/R intensity ratio represents

DOI: 10.1021/acs.jpcc.6b02246
J. Phys. Chem. C 2016, 120, 9436−9442

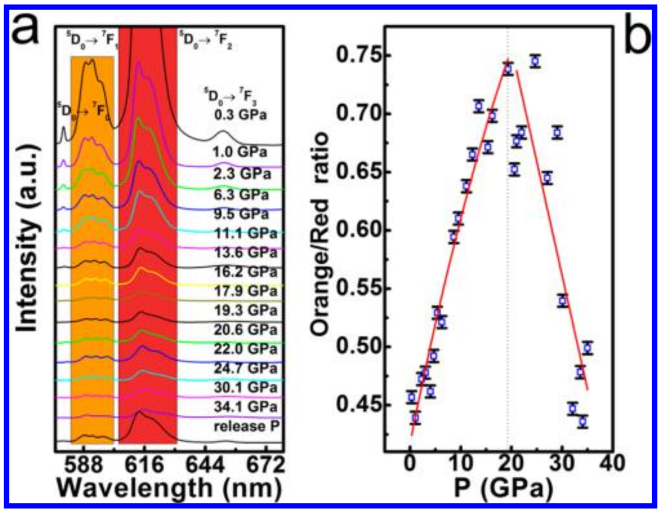

Figure 6. *In situ* PL studies of $Eu_2Sn_2O_7$ under high pressure. (a) PL spectra of $Eu_2Sn_2O_7$ between 580 and 680 nm under pressure up to 34.1 GPa. (b) Orange to red (O/R) ($^5D_0 \to {}^7F_1/{}^5D_0 \to {}^7F_2$) emission intensity ratio as a function of pressure. The red lines are the guide to the eye. Obviously, the local symmetry changes above 17.9 GPa.

the degree of local symmetry distortion around Eu^{3+} ions. With increasing pressure, the O/R ratio is increased until 17.9 GPa implying that the hexahedron EuO_8 local symmetry distortion is released with pressure. On the contrary, the O/R ratio decreases above 17.9 GPa, which indicates the local symmetry of ligands around Eu^{3+} ions is deviated from the inversion center. So, hexahedron EuO_8 is close to the perfect cubic polyhedron at 17.9 GPa. This result is in accordance with change of the free positional parameter x of O atom in the 48f site. It moves toward 0.375 for the perfect cubic symmetry. Therefore, the trigonal distortion in the SnO_6 octahedron is suppressed around 17.9 GPa, but it enhances the local symmetry distortion of EuO_8 hexahedron, which shows the complexly frustrated structure in $Eu_2Sn_2O_7$.

AC Impedance Spectroscopy at High Pressure. From in situ XRD, Raman and PL studies, it is clear to see how the lattice distortions and relaxing of both EuO_8 and SnO_6 polyhedra are evolved under high pressure. Here, ac impedance measurement is applied to investigate the evolution of the electronic states with the structural changes. Typical Nyquist plots of polycrystalline $Eu_2Sn_2O_7$ at different pressures are displayed in Figure 7a. Two semicircles are observed with increasing pressure. The arcs shift from left to right with increasing diameters below 16.6 GPa. Above that, high pressure leads to the decrease of arcs diameters. In order to analyze the impedance spectroscopy, the obtained data are usually modeled by two equivalent series circuits consisting of resistor (R) and constant phase element (CPE).[46] The CPE is expressed by the following equation and defined by two values T and P.

$$Z = 1/[T(j\omega)^P]$$

Here T is expressed in unit of capacitance component, ω and j are the frequency and the imaginary unit, respectively. A CPE is placed in parallel to a resistance so it produces a Cole element (depressed semicircle). With two series Cole circuits, it separates each of the parallel RC elements and measures their component R and C values. The total impedance has contributions from grains and grain boundaries. By fitting the data using the ZView impedance analysis software,[47] we obtain low frequency and high frequency resistance which are originated from grain and grain boundary, respectively. The grain resistance represents the intrinsic property of the studied material. The grain resistances obtained up to 30 GPa are plotted in Figure 7b. There is a 4 orders of magnitude increase in grain resistance from ambient pressure to 16.6 GPa, which implies the pressure-enhanced insulating state. With further increasing pressure, the grain resistance decreases at which the anomalous bonds change near 17.8 GPa are observed in XRD

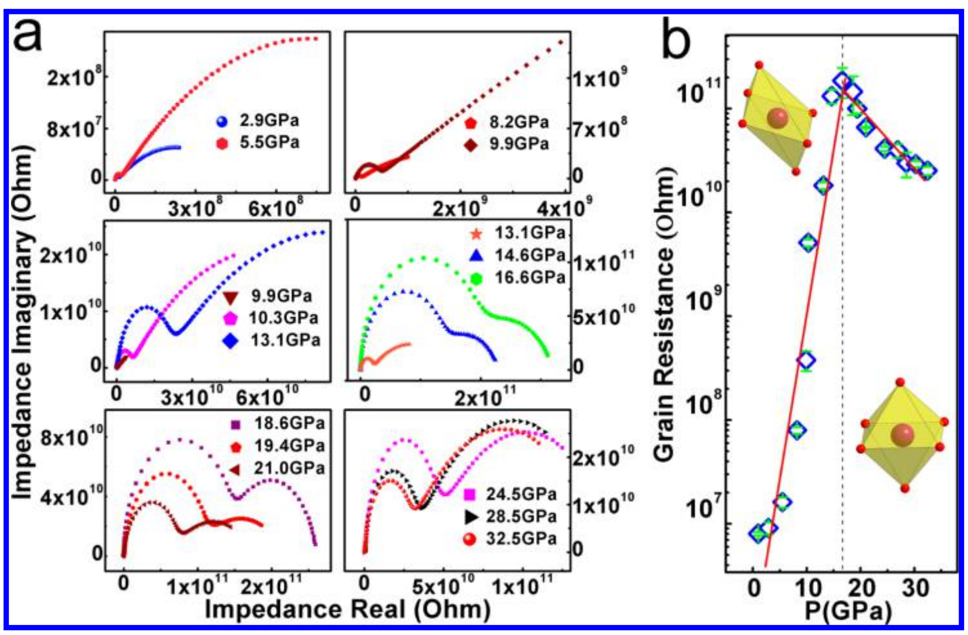

Figure 7. *In situ* high pressure AC impedance measurement of $Eu_2Sn_2O_7$ up to 32.5 GPa. (a) Nyquist plots of impedance spectroscopy. (b) Pressure dependence of grain resistance under high pressure. It shows a 4 orders of magnitude increase in grain resistance from ambient pressure to 16.6 GPa, but slightly decrease to the highest pressure. The left and right inserts in part b represent a heavily distorted SnO_6 octahedron at the transition pressure 17.8 GPa and a distortion-relaxed SnO_6 octahedron at the highest pressure 32.5 GPa.

DOI: 10.1021/acs.jpcc.6b02246
J. Phys. Chem. C 2016, 120, 9436−9442

experiment. From XRD results, the SnO_6 octahedral distortion was released near 17.8 GPa, which may induce the decrease of grain resistance. Nevertheless, this phenomenon is uncommon and only a few materials under extremely high pressure have been observed to exhibit metal to insulator transition.[48,49] It is speculated that pressure-induced trigonal lattice distortion will result in a completely opening gap at Fermi energy in this type of pyrochlore oxides. In a general scenario of crystal field splitting, the major contribution is the hybridization between the transition-metal d orbitals and the ligand oxygen 2p orbitals which influence the electronic structure.[50,51] Besides, the electronic structure near the Fermi level is sensitive with the variation in Sn−O−Sn bond angles under high pressure. Between 10.3 and 17.8 GPa, the trigonal distortion SnO_6 octahedron reaches the highest, which is described by Sn−O−Sn bending, and it leads to more insulating state as evidenced by the fact that the grain resistance increases nearly 4 orders of magnitude at higher pressure. Above 17.8 GPa, the trigonal distortion is suppressed, and meanwhile the Sn−O−Sn bond angles are toward linear configuration. So the grain resistance slight decreases to the highest pressure.

■ CONCLUSIONS

In this work, we have studied the pressure effects on structural, optical and electrical transport properties of pyrochlore $Eu_2Sn_2O_7$. Overall the pyrochlore cubic structure remains stable up to the highest pressure, but the detailed studies show that the distortions of SnO_6 and EuO_8 polyhedra induce an iso-structural transition at 17.8 GPa, where Sn−O−Sn and Eu−O−Eu bonding angle and bonding distance exhibit a kink. The bulk modulus increases 67% after this pressure, and also the Raman mode at 338 cm^{-1} related to the trigonal distortion in the SnO_6 octahedron disappears after the critical pressure. Furthermore, the anomalous luminescence of Eu^{3+} 4f−4f transition evidence the EuO_8 distortions, where the intensity ratio of orange emission (magnetic dipole) to red emission (electric dipole) shows a maximum at the 17.9 GPa. The grain-resistance increases by 4 orders of magnitude after it reaches the maximum at 16.6 GPa, and decreases slightly after the critical pressure, which leads to the enhanced insulating state.

The combined research on the structural evolution by XRD and Raman spectroscopy, and related optical and electronic transport properties under high pressure provide a comprehensive understanding of the lattice, excitation energy levels and electron configuration in this structural frustrated system. We expect that the mechanism uncovered here can provide useful guidance for the practical novel material design and synthesis with advanced properties.

■ AUTHOR INFORMATION

Corresponding Authors

*(X.W.) E-mail: xin_wang@jlu.edu.cn. Telephone: +86-431-85168881.

*(W.Y.) E-mail: wyang@carnegiescience.edu. Telephone: 1-630-252-0487.

Notes

The authors declare no competing financial interest.

■ ACKNOWLEDGMENTS

This work was financially supported by the National Natural Science Foundation of China under Grant No. 11534003 and No. 51527801, NSAF under Grant No. U1530402, and open project of State Key Laboratory of Superhard Materials (Jilin University). W.Y. acknowledges financial support from the DOE-Basic Energy Sciences (BES) X-ray Scattering Core Program (DE-FG02-99ER45775). We acknowledge Dr. Zhiqiang Chen for technical support with the high pressure experiments at the beamline BLX17C of the National Synchrotron Light Source.

■ REFERENCES

(1) Gardner, J. S.; Gingras, M. J.; Greedan, J. E. Magnetic Pyrochlore Oxides. *Rev. Mod. Phys.* **2010**, *82*, 53−107.

(2) Saha, S.; Singh, S.; Dkhil, B.; Dhar, S.; Suryanarayanan, R.; Dhalenne, G.; Revcolevschi, A.; Sood, A. Temperature-Dependent Raman and X-Ray Studies of the Spin-Ice Pyrochlore $Dy_2Ti_2O_7$ and Non-Magnetic Pyrochlore $Lu_2Ti_2O_7$. *Phys. Rev. B: Condens. Matter Mater. Phys.* **2008**, *78*, 214102.

(3) Curnoe, S. H. Structural Distortion and the Spin Liquid State in $Tb_2Ti_2O_7$. *Phys. Rev. B: Condens. Matter Mater. Phys.* **2008**, *78*, 094418.

(4) Hodges, J.; Bonville, P.; Forget, A.; Yaouanc, A.; Dalmas de Réotier, P.; André, G.; Rams, M.; Królas, K.; Ritter, C.; Gubbens, P. First-Order Transition in the Spin Dynamics of Geometrically Frustrated $Yb_2Ti_2O_7$. *Phys. Rev. Lett.* **2002**, *88*, 077204.

(5) Bonville, P.; Hodges, J.; Ocio, M.; Sanchez, J.; Vulliet, P.; Sosin, S.; Braithwaite, D. Low Temperature Magnetic Properties of Geometrically Frustrated $Gd_2Sn_2O_7$ and $Gd_2Ti_2O_7$. *J. Phys.: Condens. Matter* **2003**, *15*, 7777−7787.

(6) Malkin, B.; Lummen, T.; Van Loosdrecht, P.; Dhalenne, G.; Zakirov, A. Static Magnetic Susceptibility, Crystal Field and Exchange Interactions in Rare Earth Titanate Pyrochlores. *J. Phys.: Condens. Matter* **2010**, *22*, 276003.

(7) Kumar, R. S.; Cornelius, A. L.; Nicol, M. F.; Kam, K. C.; Cheetham, A. K.; Gardner, J. S. Pressure-Induced Structural Transitions in Tb-Pyrochlore Oxides. *Appl. Phys. Lett.* **2006**, *88*, 031903.

(8) Matsuhira, K.; Hinatsu, Y.; Tenya, K.; Amitsuka, H.; Sakakibara, T. Low-Temperature Magnetic Properties of Pyrochlore Stannates. *J. Phys. Soc. Jpn.* **2002**, *71*, 1576−1582.

(9) Zhou, H.; Wiebe, C.; Janik, J.; Balicas, L.; Yo, Y.; Qiu, Y.; Copley, J.; Gardner, J. Dynamic Spin Ice: $Pr_2Sn_2O_7$. *Phys. Rev. Lett.* **2008**, *101*, 227204.

(10) Mirebeau, I.; Apetrei, A.; Rodriguez-Carvajal, J.; Bonville, P.; Forget, A.; Colson, D.; Glazkov, V.; Sanchez, J.; Isnard, O.; Suard, E. Ordered Spin Ice State and Magnetic Fluctuations in $Tb_2Sn_2O_7$. *Phys. Rev. Lett.* **2005**, *94*, 246402.

(11) Sarte, P.; Silverstein, H.; Van Wyk, B.; Gardner, J.; Qiu, Y.; Zhou, H. D.; Wiebe, C. Absence of Long-Range Magnetic Ordering in the Pyrochlore Compound $Er_2Sn_2O_7$. *J. Phys.: Condens. Matter* **2011**, *23*, 382201.

(12) Chung, H.-Y.; Weinberger, M. B.; Levine, J. B.; Kavner, A.; Yang, J.-M.; Tolbert, S. H.; Kaner, R. B. Synthesis of Ultra-Incompressible Superhard Rhenium Diboride at Ambient Pressure. *Science* **2007**, *316*, 436−439.

(13) Shimizu, K. New Superconductors under Very High Pressure. *J. Phys.: Condens. Matter* **2007**, *19*, 125207.

(14) Fujiwara, K.; Morimoto, K.; Maeda, E.; Nishigori, S. Pressure Effect on Superconductivity in $Cd_2Re_2O_7$. *J. Phys.: Conf. Ser.* **2010**, *200*, 012043.

(15) Sakata, M.; Kagayama, T.; Shimizu, K.; Matsuhira, K.; Takagi, S.; Wakeshima, M.; Hinatsu, Y. Suppression of Metal-Insulator Transition at High Pressure and Pressure-Induced Magnetic Ordering in Pyrochlore Oxide $Nd_2Ir_2O_7$. *Phys. Rev. B: Condens. Matter Mater. Phys.* **2011**, *83*, 041102.

(16) Tafti, F. F.; Ishikawa, J. J.; McCollam, A.; Nakatsuji, S.; Julian, S. R. Pressure-Tuned Insulator to Metal Transition in $Eu_2Ir_2O_7$. *Phys. Rev. B: Condens. Matter Mater. Phys.* **2012**, *85*, 205104.

(17) Zhou, H. D.; Bramwell, S. T.; Cheng, J. G.; Wiebe, C. R.; Li, G.; Balicas, L.; Bloxsom, J. A.; Silverstein, H. J.; Zhou, J. S.; Goodenough,

DOI: 10.1021/acs.jpcc.6b02246
J. Phys. Chem. C 2016, 120, 9436−9442

J. B.; Gardner, J. S. High Pressure Route to Generate Magnetic Monopole Dimers in Spin Ice. *Nat. Commun.* **2011**, *2*, 478.

(18) Mirebeau, I.; Goncharenko, I.; Cadavez-Peres, P.; Bramwell, S.; Gingras, M.; Gardner, J. Pressure-Induced Crystallization of a Spin Liquid. *Nature* **2002**, *420*, 54−57.

(19) Saha, S.; Muthu, D. S.; Singh, S.; Dkhil, B.; Suryanarayanan, R.; Dhalenne, G.; Poswal, H.; Karmakar, S.; Sharma, S. M.; Revcolevschi, A. Low-Temperature and High-Pressure Raman and X-Ray Studies of Pyrochlore $Tb_2Ti_2O_7$: Phonon Anomalies and Possible Phase Transition. *Phys. Rev. B: Condens. Matter Mater. Phys.* **2009**, *79*, 134112.

(20) Chen, X.; Zhao, W.; Cook, R.; Liu, G. Anomalous Luminescence Dynamics of Eu^{3+} in BaFCl Microcrystals. *Phys. Rev. B: Condens. Matter Mater. Phys.* **2004**, *70*, 205122.

(21) Gong, C.; Li, Q.; Liu, R.; Hou, Y.; Wang, J.; Dong, X.; Liu, B.; Tan, X.; Liu, J.; Yang, K. Structural Phase Transition and Photoluminescence Properties of YF_3: Eu^{3+} Nanocrystals under High Pressure. *J. Phys. Chem. C* **2014**, *118*, 22739−22745.

(22) Wang, Z.; He, P.; Zhang, Y.; Li, X.; Xiong, L.; Guo, J. Photoluminescence of Y_2O_3: Eu^{3+} Prepared by Mimicking Wood Tissue. *Mater. Lett.* **2012**, *76*, 240−242.

(23) Hirano, M.; Ohmori, T. Direct Formation and Luminescence of Nanocrystals in the System $Eu_2Sn_2O_7$−$Gd_2Sn_2O_7$ Complete Solid Solutions. *J. Am. Ceram. Soc.* **2015**, *98*, 3726−3732.

(24) Fujihara, S.; Tokumo, K. Multiband Orange-Red Luminescence of Eu^{3+} Ions Based on the Pyrochlore-Structured Host Crystal. *Chem. Mater.* **2005**, *17*, 5587−5593.

(25) Zeng, J.; Wang, H.; Zhang, Y.; Zhu, M. K.; Yan, H. Hydrothermal Synthesis and Photocatalytic Properties of Pyrochlore $La_2Sn_2O_7$ Nanocubes. *J. Phys. Chem. C* **2007**, *111*, 11879−11887.

(26) Sayed, F. N.; Grover, V.; Mandal, B.; Tyagi, A. Influence of La^{3+} Substitution on Electrical and Photocatalytic Behavior of Complex $Bi_2Sn_2O_7$ Oxides. *J. Phys. Chem. C* **2013**, *117*, 10929−10938.

(27) Mao, H.; Xu, J.-A.; Bell, P. Calibration of the Ruby Pressure Gauge to 800 Kbar under Quasi-Hydrostatic Conditions. *J. Geophys. Res.* **1986**, *91*, 4673−4676.

(28) Han, Y.; Gao, C.; Ma, Y.; Liu, H.; Pan, Y.; Luo, J.; Li, M.; He, C.; Huang, X.; Zou, G. Integrated Microcircuit on a Diamond Anvil for High-Pressure Electrical Resistivity Measurement. *Appl. Phys. Lett.* **2005**, *86*, 064104.

(29) Subramanian, M.; Sleight, A.; GschneidnerJr, K.; Eyring, L. *Handbook on the Physics and Chemistry of Rare Earths*; Elsevier Science: Oxford, U.K., 1993; p 225.

(30) Yang, B.-J.; Kim, Y. B. Topological Insulators and Metal-Insulator Transition in the Pyrochlore Iridates. *Phys. Rev. B: Condens. Matter Mater. Phys.* **2010**, *82*, 085111.

(31) Larson, A.; Von Dreele, R. *General Structure Analysis System (GSAS)*; Los Alamos National Laboratory: Los Alamos, NM, 2004; Report Laur86-748.

(32) Lian, J.; Helean, K. B.; Kennedy, B. J.; Wang, L. M.; Navrotsky, A.; Ewing, R. C. Effect of Structure and Thermodynamic Stability on the Response of Lanthanide Stannate Pyrochlores to Ion Beam Irradiation. *J. Phys. Chem. B* **2006**, *110*, 2343−2350.

(33) Birch, F. Finite Elastic Strain of Cubic Crystals. *Phys. Rev.* **1947**, *71*, 809.

(34) Zhang, F. X.; Lang, M.; Liu, Z.; Ewing, R. C. Ewing. Pressure-Induced Disordering and Anomalous Lattice Expansion in $La_2Zr_2O_7$ Pyrochlore. *Phys. Rev. Lett.* **2010**, *105*, 015503.

(35) Loa, I.; Adler, P.; Grzechnik, A.; Syassen, K.; Schwarz, U.; Hanfland, M.; Rozenberg, G. K.; Gorodetsky, P.; Pasternak, M. P. Pressure-Induced Quenching of the Jahn-Teller Distortion and Insulator-to-Metal Transition in $LaMnO_3$. *Phys. Rev. Lett.* **2001**, *87*, 125501.

(36) Fischer, M.; Malcherek, T.; Bismayer, U.; Blaha, P.; Schwarz, K. Structure and Stability of $Cd_2Nb_2O_7$ and $Cd_2Ta_2O_7$ Explored by Ab Initio Calculations. *Phys. Rev. B: Condens. Matter Mater. Phys.* **2008**, *78*, 014108.

(37) Kong, L.; Karatchevtseva, I.; Blackford, M. G.; Scales, N.; Triani, G. Aqueous Chemical Synthesis of $Ln_2Sn_2O_7$ Pyrochlore Structured Ceramics. *J. Am. Ceram. Soc.* **2013**, *96*, 2994−3000.

(38) Vandenborre, M.; Husson, E.; Chatry, J.; Michel, D. Rare-Earth Titanates and Stannates of Pyrochlore Structure; Vibrational Spectra and Force Fields. *J. Raman Spectrosc.* **1983**, *14*, 63−71.

(39) Gupta, H.; Brown, S.; Rani, N.; Gohel, V. A Lattice Dynamical Investigation of the Raman and the Infrared Frequencies of the Cubic $A_2Sn_2O_7$ Pyrochlores. *Int. J. Inorg. Mater.* **2001**, *3*, 983−986.

(40) Arenas, D.; Gasparov, L.; Qiu, W.; Nino, J.; Patterson, C.; Tanner, D. Raman Study of Phonon Modes in Bismuth Pyrochlores. *Phys. Rev. B: Condens. Matter Mater. Phys.* **2010**, *82*, 214302.

(41) Seibald, M.; Rosenthal, T.; Oeckler, O.; Maak, C.; Tücks, A.; Schmidt, P. J.; Wiechert, D.; Schnick, W. New Polymorph of the Highly Efficient Led-Phosphor $SrSi_2O_2N_2$:Eu^{2+} Polytypism of a Layered Oxonitridosilicate. *Chem. Mater.* **2013**, *25*, 1852−1857.

(42) Fu, Z.; Yang, H. K.; Moon, B. K.; Choi, B. C.; Jeong, J. H. La2sn2o7: Eu^{3+} Micronanospheres: Hydrothermal Synthesis and Luminescent Properties. *Cryst. Growth Des.* **2009**, *9*, 616−621.

(43) Chen, R.; Shen, Y.; Xiao, F.; Liu, B.; Gurzadyan, G.; Dong, Z. L.; Sun, X. W.; Sun, H. Surface Eu-Treated Zno Nanowires with Efficient Red Emission. *J. Phys. Chem. C* **2010**, *114*, 18081−18084.

(44) Su, Y.; Peng, L.; Du, C.; Wang, X. Controllable Synthesis of Undoped and Doped Calcium Niobate Nanocrystals for Tailored Structural, Electronic, and Luminescent Properties. *J. Phys. Chem. C* **2012**, *116*, 15−21.

(45) Zeng, Q.; Ding, Z.; Zhang, Z.; Sheng, Y. Photoluminescence and Raman Spectroscopy Studies of $Eu(OH)_3$ Rods at High Pressures. *J. Phys. Chem. C* **2010**, *114*, 4895−4900.

(46) Sinclair, D. C.; West, A. R. Impedance and Modulus Spectroscopy of Semiconducting Batio3 Showing Positive Temperature Coefficient of Resistance. *J. Appl. Phys.* **1989**, *66*, 3850−3856.

(47) Johnson, D. *Zview: A Software Program for Ies Analysis*, Version 2.8; Scribner Associates. Inc.: Southern Pines, NC, 2008; p 200.

(48) Korneta, O.; Chikara, S.; Parkin, S.; DeLong, L.; Schlottmann, P.; Cao, G. Pressure-Induced Insulating State in $Ba_{1-x}R_xIrO_3$ (R= Gd, Eu) Single Crystals. *Phys. Rev. B: Condens. Matter Mater. Phys.* **2010**, *81*, 045101.

(49) Matsuoka, T.; Shimizu, K. Direct Observation of a Pressure-Induced Metal-to-Semiconductor Transition in Lithium. *Nature* **2009**, *458*, 186−189.

(50) Okamoto, J.; Mizokawa, T.; Fujimori, A.; Takeda, T.; Kanno, R.; Ishii, F.; Oguchi, T. Photoemission Study of Electronic Structure and Metal-Semiconductor Transition in Pyrochlore-Type Tl_2 Ru_2O_7. *Phys. Rev. B: Condens. Matter Mater. Phys.* **2004**, *69*, 035115.

(51) Mizoguchi, H.; Eng, H. W.; Woodward, P. M. Probing the Electronic Structures of Ternary Perovskite and Pyrochlore Oxides Containing Sn^{4+} or Sb^{5+}. *Inorg. Chem.* **2004**, *43*, 1667−1680.

DOI: 10.1021/acs.jpcc.6b02246
J. Phys. Chem. C 2016, 120, 9436−9442